CW Operation of a Tunable 1550 nm VCSEL Integrating Liquid-Crystal Microcells

B. Boisnard, C. Levallois, C. Paranthoen, S. Pes, T. Camps, B. Sadani, K. Tavernier, S. Bouchoule, L. Dupont, M. Alouini, P. Debernardi and V. Bardinal

***Abstract*—An InP based Vertical Cavity Surface Emitting Laser (VCSEL) associated with a liquid crystal (LC) microcell monolithically integrated on its surface for spectral tuning is investigated. Unlike tunable VCSELs integrating a movable membrane, here the physical length of the cavity remains unchanged and only the voltage applied on the LC ensures a refractive index modification for a particular polarization emitted by the VCSEL. This tunable VCSEL operates in CW at room temperature and exhibits more than 23 nm wavelength tuning around 1.55 µm with a maximum applied voltage of 20V. The measured laser threshold around 6.5 mW is still comparable to VCSEL without LC microcell, a clear indication that the optical losses related the LC are very low. On the other hand, for this first optically pumped device, the lasing characteristics suggest that the LC birefringence is lower than expected. To assess this hypothesis, thermal-optical simulations have been conducted.**

***Index Terms*— Vertical cavity surface emitting lasers, Liquid crystal devices, Semiconductor lasers.**

I. Introduction

VERTICAL-CAVITY Surface-Emitting Lasers (VCSELs) are key optical sources for optical communications, and more recently for applications like autofocus imaging or facial recognition on smartphones [1]. Their well-known advantages related to longitudinal single-mode emission, circular beam shape with a low divergence, low-power consumption, and an easy 2D integration for a mass production are very attractive for such applications. However, for a wider range of applications, including gas sensing [2], Optical Coherence Tomography (OCT) [3],[4], Fiber Bragg Grating (FBG) sensing [5] and optical spectroscopy [6], wavelength tunability is required. In this case, the large free spectral range related to the VCSEL microcavity becomes interesting to obtain a wide spectral tunability without mode hopping. To realize such tunable VCSEL, it is then required to change the optical length of the cavity. The most used technique is based on the variation of the physical length of the optical resonator. This is typically achieved by thermal or electrostatic actuation of a suspended membrane acting as a movable end mirror for the cavity, which is usually fabricated by using micro electrical-mechanical systems (MEMS) technology. Broadband wavelength tunability has already been demonstrated using this technique, and mainly for MEMS-VCSEL operating at wavelengths ranging from 850 nm [7] to 1550 nm [8]. These demonstrations have been both performed with optically [9],[10] and electrically pumped devices [2]-[8]. However, low-cost MEMS-VCSELs are not available yet in the market, probably in relation to their fabrication complexity or the robustness of their membranes. Recently, a MEMS structure based on a more robust design has been investigated [11], but as for other MEMS-VCSEL, weaknesses can be raised concerning the linewidth and stability of the emitted wavelength [12], [13].

A promising alternative to this MEMS approach is the use of liquid crystal (LC) which can provide a large refractive index tuning with a moderate driving voltage and very low power consumption. Several demonstrations have been conducted in the past to combine LC within compact photonic devices such as ring resonators [14], photodiodes [15] or VCSEL [16]. However, there is only one demonstration reporting the use of LC inside a VCSEL cavity in order to tune its wavelength [17]. In this pioneering work, a macro-sized LC cell with unperfected thickness control of the LC led unfortunately to lasing operation in a pulsed regime only. More recently, simulations results have been published on a 1.55 µm-VCSEL designed with nematic LC enclosed within the VCSEL cavity showing that a tuning range of 68 nm might be expected [18].

In this paper, we report for the first time a CW operation at room temperature (RT) of a tunable VCSEL emitting at 1550 nm integrating a LC microcell monolithically fabricated on an InP based half-cavity VCSEL. The design and fabrication steps are detailed. Laser characterizations are also presented, discussed and compared to thermal-optical simulations.

Submission date: December xx, 2019

The authors acknowledge RENATECH / RENATECH+ (the French national network of facilities for micronanotechnology) with LAAS-CNRS, C2N-CNRS/UPSUD and NanoRennes for technological support. The Direction Générale de l'Armement (DGA) and the French National Research Agency (ANR) are acknowledged for financial support (ANR-14-ASTR-0007 HYPOCAMP and ANR-15-CE19-0012 DOCT VCSEL).

B. Boisnard, T. Camps, B. Sadani and V. Bardinal are with Univ Toulouse, CNRS, LAAS, 7 Ave Colonel Roche, F-31400 Toulouse, France. (e-mail: bardinal@laas.fr).

C. Levallois, C. Paranthoen, S. Pes, K. Tavernier and M. Alouini are with Univ Rennes, INSA Rennes, CNRS, Institut FOTON – UMR 6082, F-35000 Rennes, France. (e-mail: Christophe.Levallois@insa-rennes.fr).

S. Bouchoule is with C2N (Centre for Nanoscience and nanotechnology), CNRS, Université Paris-Sud, 91360 Marcoussis, France. (e-mail: sophie.bouchoule@c2n.upsaclay.fr)

L. Dupont is with IMT Atlantique, Optics Department, 655 Avenue du Technopôle, 29200 Plouzané, France. (e-mail: laurent.dupont@imt-atlantique.fr).

P. Debernardi is with Consiglio Nazionale delle Ricerche (CNR), IEIIT, 10129 Torino, Italy (e-mail: pierluigi.debernardi@ieiit.cnr.it).

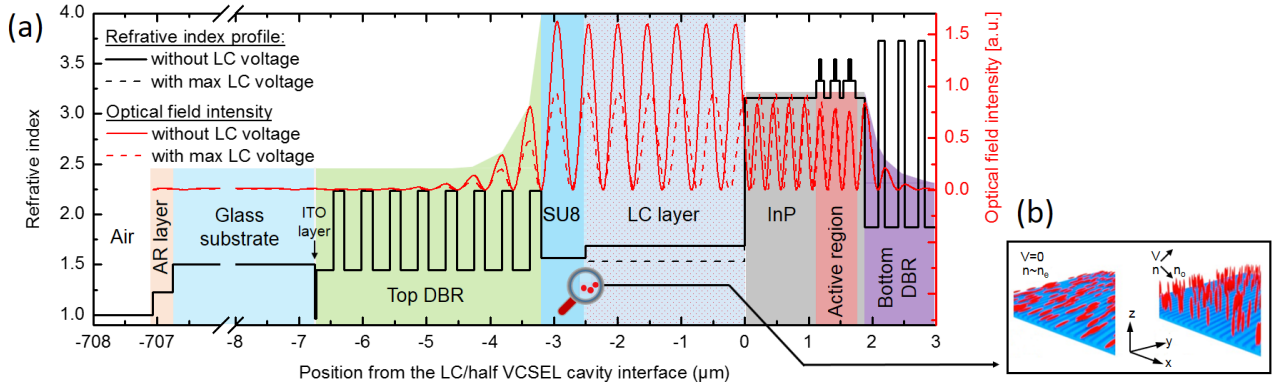

Fig. 1. (a) LC-VCSEL structure and internal optical field intensity for resonant modes related to the extraordinary index for two different voltages applied on the LC layer. (b) Enlarged schematic view of the subwavelength gratings printed on the SU8 layer for the LC alignment and the LC molecules reorientation when AC voltage applied on the LC microcells is maximum.

II. Design and Technology

Our tunable device consists in micro-sized LC cell monolithically integrated above an InP based half-VCSEL. For this first realization of a CW LC-VCSEL operating at RT, the semiconductor part of the cavity has been designed for optical pumping to simplify the fabrication process as much as possible. The active region consists in 9 strained InGaAsP quantum wells (QWs) grown by gas source molecular beam epitaxy on InP(001) substrate. These QWs, emitting at 1.55 µm, are distributed over three optical standing wave anti-node positions in the cavity. The bottom mirror is a 5×(SiN_x/aSi) periods completed by a gold layer deposited by sputtering to reach a theoretical reflectivity from the inner cavity of 99.7%. This stack of layers is transferred onto a Si substrate by a polymer bonding using a 3 µm thick BCB layer. Then the InP substrate is removed by mechanical thinning and chemical etching to obtain the half-VCSEL. The refractive index profile as well as the resonant stationary field inside the half-VCSEL cavity are depicted in Fig. 1.

The technological process then continues with the collective fabrication of LC microcells monolithically integrated onto the half VCSEL surface derived from a method based on dry thick resist films [19]. First, a thick UV negative photoresist (MicroChem PermiNex 2000) is spin-coated on the sample and exposed through a mask to define square areas, which will be filled by LC in the final processing steps. Those microcells are then covered by a top DBR with a theoretical reflectivity of 99.5%, consisting of 8×(SiO_2/TiO_2) periods deposited on a glass substrate, previously coated with a 23 nm ITO electrode to apply the voltage on the LC microcells. This upper part of the device, covered by an antireflection layer at 1.55 µm, is then sealed to the top surface of the half-VCSEL at a low temperature (150°C). Prior to this step, the top mirror surface is prepared for further LC molecules alignment. This alignment is obtained through a planar anchoring on a sub-wavelength grating printed on a 600 nm-thick SU8 layer before the sealing. Reference [19] provides details about this part of the process. The sub-wavelength grating is ensured by a well-controlled nanoimprint process to define a period of 780 nm, a duty cycle of 50:50, and a depth in the range of [70-80 nm]. This grating schematically depicted as a blue layer in Fig. 1(b), has been designed to allow an efficient orientation of the LC molecules during the microcells filling while limiting optical losses by diffraction at the wavelength of 1.55 µm.

The final step consists in filling under vacuum the microcells by a nematic LC similar to E7. This filling is achieved at a temperature higher than the nematic-isotropic transition (70 °C) thanks to lateral apertures previously defined in the PermiNex photoresist. All the layers and their associated refractive indices are represented in Fig. 1. The distribution of the stationary field inside the VCSEL cavity is also illustrated for both cases, without applied voltage and for maximum applied voltage, i.e. when all the LC molecules are reoriented. As illustrated Fig. 1(b), without voltage, the average orientation of the LC molecules (i.e. the director) is parallel to the surface, and the refractive index is maximum (close to the extraordinary index, n_e). As the applied voltage increases, the director is reoriented and the refractive index decreases towards n_0 (the ordinary index) leading to a blue shift for the resonant wavelength. To avoid polarization bistability in the VCSEL, attention has been to the cavity design. In particular, the LC thickness has been adjusted in order to reject the resonant modes related to n_0 (being not affected by the applied voltage) far from the maximum gain of the QWs, while keeping a resonant mode related to n_e centered in the spectral window emitted by the QWs. The resonant mode with a linear polarization parallel (or perpendicular) to the director will be referred to as "EM for extraordinary mode" (or "OM for ordinary mode") in the followings.

III. Results and Discussion

After the fabrication stage, the tunable VCSEL has been placed on a Peltier thermoelectric Cooler and characterized under optical pumping using a CW 980 nm semiconductor fibered laser diode focused on a 15 µm diameter spot ($1/e^2$ waist size). Fig. 2 shows the VCSEL output power as a function of the absorbed pump power measured for different voltages applied on the LC microcells. As shown in Fig. 2, the tunable VCSEL exhibits a CW operation at 17°C with a threshold power at around 6.5 mW. This threshold is not strongly dependent on the applied voltage and corresponds to a threshold power density of few $kW.cm^{-2}$, very close to the ones previously reported for equivalent VCSELs incorporating no LC [20].

Thus, as expected and demonstrated in previous works [15], [19], the presence of the LC leads to negligible additional losses, even in such highly sensitive VCSEL structure. However, this LC layer has a significant impact on the spectral behavior of the VCSEL emission. As illustrated in Fig. 2, below 8 mW the VCSEL emission is polarized accordingly to the EM, while above 8 mW a polarization bistability from EM to OM appears. Finally, beyond the thermal roll-over, the OM becomes dominant.

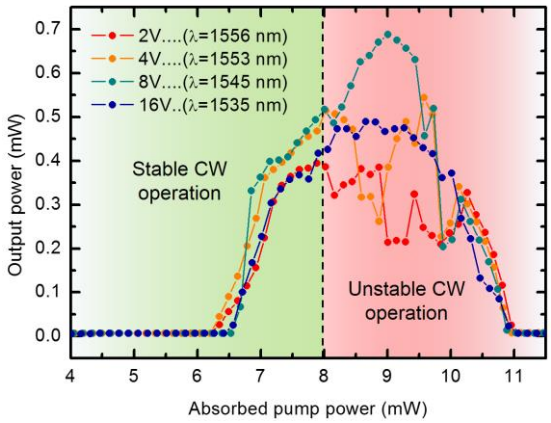

Fig. 2. Output power emitted as a function of the absorbed pump power for different AC voltages (20 kHz) applied on the LC microcells.

Consequently, the tuning range has been measured for a pump power to 7.8 mW at the upper limit of the stability area, for a laser emission exclusively set on an EM. With such a pump power, the output power is comprised between 0.35 mW and 0.5 mW for applied voltages in the 0V-16V range. Fig. 3 represents lasing spectra recorded for LC voltages ranging from 0V to 20V. Without any applied voltage on the LC, the lasing wavelength is centered at 1556.5 nm, and is blue-shifted continuously down to 1533.1 nm when the voltage is increased to 20V, leading to an available tuning range of 23.5 nm.

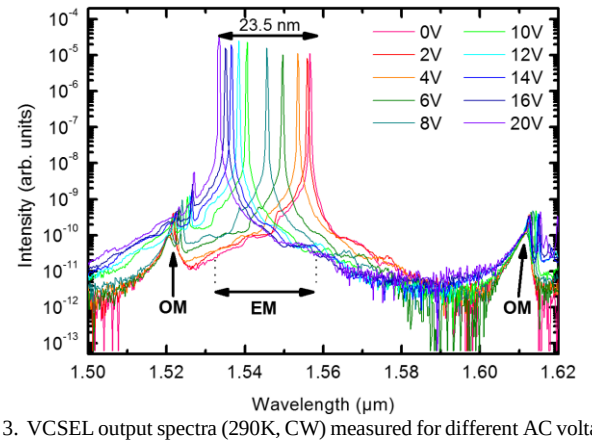

Fig. 3. VCSEL output spectra (290K, CW) measured for different AC voltages (20 kHz) applied on the LC and at a constant pump power set just below the unstable operation area (7.8 mW). The arrows give the spectral positions of the tunable lasing EM and the non-lasing OM corresponding respectively to the extraordinary (n_e) and ordinary (n_0) refractive indices of the LC.

This blue-shift of the lasing wavelength related to the EM is consistent with the fact that n_e decreases with the applied electric field on the LC layer. The wavelength shift starts at 2V with a tuning efficiency close to 2 nm/V between 2V and 10V, which decreases to 0.7 nm/V above 10V when most LC molecules have been reoriented along the applied electric field. For higher voltages than 20V the EM does not shift anymore which means that n_e has decreased but never reaches the n_0 value. Also, as indicated in Fig. 3, two peaks identified as being OM are located at 1521.6 nm and 1612.3 nm. These peaks are respectfully red-shifted by 5.4 nm and 3.2 nm when the voltage is increased, red-shifting being even more pronounced for high voltages when the OM and EM become closer. To explain this uncommon behavior, as OM are expected to be independent of the voltage applied on the LC layer, additional simulations have been conducted.

For this first proof of concept, the thermal resistance has not been optimized. The thick InP layer (1.15 µm) which is transparent at the pump wavelength does not offer a strong thermal insulation between LC and the heated active region of the VCSEL. Furthermore, the employed bonding method to report III-V active region on a Si substrate by using BCB polymer is not the best approach to minimize the thermal resistance of the VCSEL. In the following, a more advanced modeling integrating the dependence of LC birefringence properties with respect to temperature has been undertaken to evaluate how the rise in temperature can affect the tuning range. To that end, the wavelength dependence of OM and EM, have been extracted from Fig. 3 and reported in Fig.4(a). For the modelling input parameters, such as the SU8 thickness, the LC microcell thickness and the LC refractive index, we consider slight variations with regards to nominal value, mainly because they not be accurately known. For the two thicknesses, being 600 and 2300 nm respectively, we have assumed a ±150 nm tolerance, considering some processing deviations. These two thicknesses were thus set as free parameters within the ±150 nm deviation to fit the experimental results. For the LC refractive index, we use the experimental tuning curves (circles and squares in Fig. 4(a)) and the nearly linear dependence of the resonant wavelength with the index, to extract the LC indices, and consider the following phenomenological voltage dependence [x?]: ~~$n = n_0 + \left[1 + \cos\frac{\pi V}{V_{max}}\right].\frac{dn}{2}$~~ *krassimir's formula instead ?* Relying on [21], we also consider in our model the thermal degradation of our nematic LC, giving rise to typical LC indexes variations with voltage as presented in Fig. 4(b).

The lower bound of the extraordinary index does not reach its ideal value (n_0) and it can be attributed to a portion of inactive LC molecules that do not react to the applied voltage. In the following simulations, we apply a modified 1D-TMM (transfer matrix method) code, where the LC grating effect is taken into account using a Rigorous Couple Wave Analysis (RCWA). RCWA allows computing the transmission matrix of the grating, which is otherwise analytical for the entire layer stack. The 1D code is applied for n_0 and n_e providing the resonant wavelengths, QW material gain, and the corresponding standing wave profile for each resonant wavelength (see Fig. 1). The OM gain is computed mainly to check that OM experiences a higher threshold, and thus to ensure that EM is the lasing mode as requested. This is confirmed after a preliminary parametric investigation of the

effect of SU8 and microcell thicknesses, as shown in Fig 4(c). A thickness value of 700 nm is found for the SU8 layer, and as illustrated in Fig 4(a), with a fine variation of the microcell thickness experimental results are well reproduced. Other combinations of SU8 and LC thicknesses provide either a wrong wavelength or a mode hopping towards a wavelength where a lower lasing threshold is found (see Fig. 4(c)). Thus, satisfactory matching between experiment and simulation is found for SU8/LC thicknesses of 700 and 2180 nm, respectively. Finally, the index variation is supposed to be swept between 1.68 and 1.55, indicating an efficiency degradation in comparison with the nominal range of 1.72-1.52 expected for our nematic LC. This reduction in the LC birefringence, and thus in the wavelength tuning is mainly attributed to its thermal dependence leading to a collapse of the LC birefringence around 60°C. Accordingly, the use of a nematic QYPDL-HD002 LC is expected to provide a higher tuning range, close to 45 nm as illustrated in Fig. 4(d).

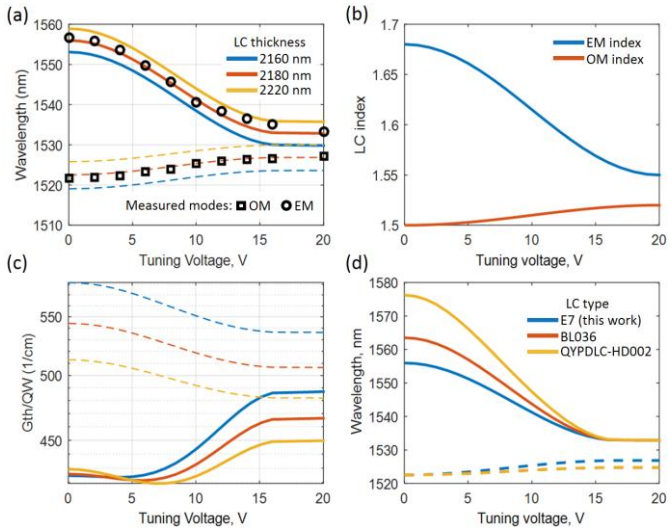

Fig. 4. (a) Computed wavelength emission of the EM/OM (continuous/dashed lines) vs. voltage for three different LC reservoir thicknesses (see legend). Open squares and circles refer to the experimental results from Fig. 2. (b) Phenomenological LC index dependence on applied voltage. (c) Threshold gain corresponding to tuning curves of Fig. 4(a). (d) Similar to (a), but with different LC types (see legend).

IV. Conclusion

A 1.55 µm InP-VCSEL with CW operation at RT and 23.5 nm wavelength tunability has been designed, fabricated and characterized. This device combines InP based materials with LC microcells collectively fabricated and integrated on the surface of a half-cavity VCSEL. The maximum driving voltage applied to the LC is 20V without any apparent current, leading to low power consumption for the wavelength control of the device. In addition, simulations based on the experimental results have been conducted to identify the discrepancy between expected and observed spectra behaviors. It turns out that, the appearing reduction of LC birefringence is induced by thermal conduction between the active medium and the LC microcell. Finally, by using LC with a better thermal tolerance larger tuning ranges are expected. Further work includes investigation of the dynamical behavior of wavelength tuning. Indeed, typical response time of such LC being in the millisecond range, a frequency chirp of 4THz/ms could be reached for coherent Lidar applications.

References

[1] J. Skidmore, 'Semiconductor Lasers for 3-D Sensing', *Optics and Photonics News*, vol. 30, pp. 26–33, Feb-2019.

[2] B. Kogel *et al.*, 'Simultaneous Spectroscopy of NH3 and CO Using a 50nm Continuously Tunable MEMS-VCSEL', *IEEE Sens. J.*, vol. 7, no. 11, pp. 1483–1489, Nov. 2007.

[3] B. Potsaid, V. Jayaraman, J. G. Fujimoto, J. Jiang, P. J. S. Heim, and A. E. Cable, 'MEMS tunable VCSEL light source for ultrahigh speed 60kHz - 1MHz axial scan rate and long range centimeter class OCT imaging', presented at the SPIE BiOS, San Francisco, California, USA, 2012, p. 82130M.

[4] D. D. John *et al.*, 'Wideband Electrically Pumped 1050-nm MEMS-Tunable VCSEL for Ophthalmic Imaging', *J. Light. Technol.*, vol. 33, no. 16, pp. 3461–3468, Aug. 2015.

[5] C. F. R. Mateus and C. L. Barbosa, 'Harsh environment temperature and strain sensor using tunable VCSEL and multiple fiber bragg gratings', 2007, pp. 496–498.

[6] V. J. Kitsmiller, M. M. Dummer, K. Johnson, G. D. Cole, and T. D. O'Sullivan, 'Frequency domain diffuse optical spectroscopy with a near-infrared tunable vertical cavity surface emitting laser', *Opt. Express*, vol. 26, no. 16, p. 21033, Aug. 2018.

[7] D. D. John *et al.*, 'Single-Mode and High-Speed 850nm MEMS-VCSEL', in *Lasers Congress 2016 (ASSL, LSC, LAC)*, Boston, Massachusetts, 2016, p. ATh5A.2.

[8] C. Gierl *et al.*, 'Surface micromachined tunable 155 µm-VCSEL with 102 nm continuous single-mode tuning', *Opt. Express*, vol. 19, no. 18, p. 17336, Aug. 2011.

[9] V. Jayaraman, G. D. Cole, M. Robertson, A. Uddin, and A. Cable, 'High-sweep-rate 1310 nm MEMS-VCSEL with 150 nm continuous tuning range', *Electron. Lett.*, vol. 48, no. 14, p. 867, 2012.

[10] V. Jayaraman *et al.*, 'Rapidly swept, ultra-widely-tunable 1060 nm MEMS-VCSELs', *Electron. Lett.*, vol. 48, no. 21, p. 1331, 2012.

[11] H. K. Sahoo *et al.*, 'Tunable MEMS VCSEL on Silicon Substrate', *IEEE J. Sel. Top. Quantum Electron.*, vol. 25, no. 6, pp. 1–7, Nov. 2019.

[12] H. Halbritter, C. Sydlo, B. Kogel, F. Riemenschneider, H. L. Hartnagel, and P. Meissner, 'Impact of Micromechanics on the Linewidth and Chirp Performance of MEMS-VCSELs', *IEEE J. Sel. Top. Quantum Electron.*, vol. 13, no. 2, pp. 367–373, 2007.

[13] S. Paul *et al.*, 'Far-field, linewidth and thermal characteristics of a high-speed 1550-nm MEMS tunable VCSEL', *Opt. Express*, vol. 24, no. 12, p. 13142, Jun. 2016.

[14] W. D. Cort, J. Beeckman, T. Claes, K. Neyts, and R. Baets, 'Wide tuning of silicon-on-insulator ring resonators with a liquid crystal cladding', *Opt. Lett.*, vol. 36, no. 19, pp. 3876–3878, Oct. 2011.

[15] C. Levallois *et al.*, 'Liquid crystal-based tunable photodetector operating in the telecom C-band', *Opt. Express*, vol. 26, no. 20, p. 25952, Oct. 2018.

[16] Y. Xie, J. Beeckman, W. Woestenborghs, K. Panajotov, and K. Neyts, 'VCSEL With Photo-Aligned Liquid Crystal Overlay', *IEEE Photonics Technol. Lett.*, vol. 24, no. 17, pp. 1509–1512, Sep. 2012.

[17] O. Castany, L. Dupont, A. Shuaib, J. P. Gauthier, C. Levallois, and C. Paranthoën, 'Tunable semiconductor vertical-cavity surface-emitting laser with an intracavity liquid crystal layer', *Appl. Phys. Lett.*, vol. 98, no. 16, p. 161105, 2011.

[18] L. Frasunkiewicz, T. Czyszanowski, H. Thienpont, and K. Panajotov, 'Electrically tunable VCSEL with intra-cavity liquid crystal: Design, optimization, and analysis of polarization- and mode-stability', *Opt. Commun.*, vol. 427, pp. 271–277, Nov. 2018.

[19] B. Sadani *et al.*, 'Liquid-Crystal Alignment by a Nanoimprinted Grating for Wafer-Scale Fabrication of Tunable Devices', *IEEE Photonics Technol. Lett.*, vol. 30, no. 15, pp. 1388–1391, Aug. 2018.

[20] F. Taleb *et al.*, 'Enhancement of VCSEL Performances Using Localized Copper Bonding Through Silicon Vias', *IEEE Photonics Technol. Lett.*, vol. 29, no. 13, pp. 1105–1108, Jul. 2017.

[21] J. Li, S.-T. Wu, S. Brugioni, R. Meucci, and S. Faetti, 'Infrared refractive indices of liquid crystals', *J. Appl. Phys.*, vol. 97, no. 7, p. 073501, Apr. 2005.